SCIENCE CHINA
Chemistry

• ARTICLES •

November 2016 Vol.59 No.11:1479–1485
doi: 10.1007/s11426-016-0109-1

High capacity lithium-manganese-nickel-oxide composite cathodes with low irreversible capacity loss and good cycle life for lithium ion batteries

Jingwen Zhang, Xun Guo, Sumei Yao & Xinping Qiu*

Key Lab of Organic Optoelectronics and Molecular Engineering, Department of Chemistry, Tsinghua University, Beijing 100084, China

Received March 14, 2016; accepted April 28, 2016; published online September 23, 2016

We report a method to eliminate the irreversible capacity of $0.4Li_2MnO_3{\cdot}0.6LiNi_{0.5}Mn_{0.5}O_2$ ($Li_{1.17}Ni_{0.25}Mn_{0.583}O_2$) by decreasing lithium content to yield integrated layered-spinel structures. XRD patterns, High-resolution TEM image and electrochemical cycling of the materials in lithium cells revealed features consistent with the presence of spinel phase within the materials. When discharged to about 2.8 V, the spinel phase of LiM_2O_4 (M=Ni,Mn) can transform to rock-salt phase of $Li_2M_2O_4$ (M=Ni,Mn) during which the tetravalent manganese ions are reduced to an oxidation state of 3.0. So the spinel phase can act as a host to insert back the extracted lithium ions (from the layered matrix) that could not embed back into the layered lattice to eliminate the irreversible capacity loss and increase the discharge capacity. Their electrochemical properties at room temperature showed a high capacity (about 275 mAh g^{-1} at 0.1 C) and exhibited good cycling performance.

Lithium ion electrode, composite materials, Lithium-rich material, spinel phase, layered phase

Citation: Zhang J, Guo X, Yao S, Qiu X. High capacity lithium-manganese-nickel-oxide composite cathodes with low irreversible capacity loss and good cycle life for lithium ion batteries. *Sci China Chem*, 2016, 59: 1479–1485, doi: 10.1007/s11426-016-0109-1

1 Introduction

Recently, composite lithium and manganese-rich $xLi_2MnO_3{\cdot}(1-x)LiMO_2$ compounds (M=Mn, Ni, Co) have attracted much attention due to their high capacity of 250 mAh g^{-1} and good structural stability [1–6], compared to the commercialized cathode materials (eg. $LiCoO_2$, $LiMn_2O_4$ and $LiFePO_4$). These materials have been described as a 'solid solution' $Li[Li_xM_{1-x}]O_2$, which is a single-phase material with *C2/m* symmetry and exhibits significant ordering between Li^+ and the transition metal [7]. At the same time, they have also been presented as a two-component composite structure $xLi_2MnO_3{\cdot}(1-x)LiMO_2$ (M = Mn, Ni, Co), in which Li_2MnO_3 and $LiMO_2$ exit in short-range order [8–10]. As a result, much debate has been spurred over the atomic structure of these materials and how they relate to the electrochemical properties. During the initial charge, lithium extracts from the Li_2MnO_3 component ($Li_2O{\cdot}MnO_2$) with a simultaneous release of oxygen above 4.5 V, which results in a net loss of Li_2O to yield MnO_2, and the new component of MnO_2 is electrochemically active in the electrode structure increasing the discharge specific capacity [11,12]. In this respect, two lithium ions extract from the Li_2MnO_3 component during the first charge, while only one lithium per MnO_2 unit embeds into the lattice during first discharge. So these materials undergo a huge irreversible capacity loss in the first cycle.

Some efforts have been made to lower irreversible capacity loss in the first cycle such as mild acid treatment and surface modification. It was found that Li^+ can be removed from $xLi_2MnO_3{\cdot}(1-x)LiMO_2$ (M=Mn, Ni, Co) by

*Corresponding author. E-mail: qiuxp@tsinghua.edu.cn

mild acid treatment [13–16]. Kang *et al*. [17] demonstrated that xLi$_2$MnO$_3$·(1–x)LiMO$_2$ electrodes operate with 100% coulombic efficiency after acid treatment with 0.1 mol L^{-1} HNO$_3$ (initial PH≈1.0). Despite the effectiveness of the method to reduce the first cycle irreversible capacity loss, the acid treatment may damage the structure as a result of possible H$^+$ - Li$^+$ exchange or etching/dissolution reactions at the surface, which results in the poor cycle life performance [18]. Surface modification, with inert compounds such as Al$_2$O$_3$, Nb$_2$O$_5$, Ta$_2$O$_5$, ZrO$_2$, TiO$_2$, ZnO, Al(OH)$_3$ and AlPO$_4$, lowers the surface reactivity of charged electrode particles to provide robust surfaces and structures that can withstand the harsh chemical and electrochemical environments. These attempts help to reduce the irreversible capacity loss, but that could not eliminate the irreversible capacity loss completely [19–23]. Spherical Li[Li$_{0.2}$Mn$_{0.54}$Ni$_{0.13}$Co$_{0.13}$]O$_2$ material was treated with Na$_2$S$_2$O$_8$ to increase the coulombic efficiency of the first cycle, that is attributed to the formation of spinel phase on the surface of the material and the extraction of lithium and oxygen [24]. Another strategy to make the irreversible capacity loss to 0 mAh g^{-1} is to blend the Li-rich materials with Li-free insertion hosts such as V$_2$O$_5$, VO$_2$, LiV$_3$O$_8$, Li$_4$Mn$_5$O$_{12}$ [25–27]. However, these technologies are too complicated, and it is necessary to search for simple methods. The spinel typed Li-M-Os, such as LiMn$_2$O$_4$ and LiNi$_{0.5}$Mn$_{1.5}$O$_4$, have been studied extensively because of low cost and high safety [28,29].

Here, we report a method to eliminate the irreversible capacity by decreasing lithium content of 0.4Li$_2$MnO$_3$·0.6LiNi$_{0.5}$Mn$_{0.5}$O$_2$ (Li$_{1.17}$Ni$_{0.25}$Mn$_{0.583}$O$_2$) to yield integrated layered-spinel structures. When discharged to about 2.8 V, the spinel phase of LiM$_2$O$_4$ (M=Mnor Ni$_{0.5}$Mn$_{1.5}$) can transform to rock-salt phase of Li$_2$M$_2$O$_4$ (M=Mn or Ni$_{0.5}$Mn$_{1.5}$) during which the tetravalent manganese ions are reduced to an oxidation state of 3.0. So the spinel phase can act as a host to insert back the extracted lithium ions (from the layered matrix) that could not embed back into the layered lattice to eliminate the irreversible capacity loss and increase the discharge capacity. Their electrochemical properties at room temperature showed a high capacity (about 275 mAh g^{-1} at 0.1 C) and exhibited good cycling performance.

2 Experimental

Nickel nitrate hexahydrate (Ni(NO$_3$)$_2$·6H$_2$O), manganese sulfate monohydrate (MnSO$_4$·H$_2$O), urea (CO(NH$_2$)$_2$), and lithium carbonate (Li$_2$CO$_3$) were used as the starting materials. The precursors were prepared as follows: Ni(NO$_3$)$_2$·6H$_2$O and MnSO$_4$·H$_2$O (cationic ratio of Ni:Mn=2:3) were dissolved in deionized water. At the same time, some urea was added to the metal solution after rigorous stirring to form a clear solution. Then, the solution was placed into a Teflon-lined stainless steel autoclave and heated at 200 °C for 6 hours. Collected samples were filtered, washed, and dried at 100 °C over 24 h. The obtained Ni$_{0.4}$Mn$_{0.6}$CO$_3$ and Li$_2$CO$_3$ were mixed thoroughly, and the mixture was first heated at 500 °C for 5 h in air, and then calcinated at 800 °C or 900 °C for 24 h in air to obtain the cathode material, which was quenched in air.

X-ray diffraction (XRD, D8 advance XRD diffractometer , Bruker Corporation, Germany) was performed on a D8 Advance Bruker diffractometer, with a Cu Kα radiation source (λ=1.5406Å). The morphology of the materials was observed by the scanning electron microscope (SEM, S-4500 SEM, Hitachi Corporation, Japan). The high-resolution TEM images of the powders were collected on a JEOL model JEM-2010 transmission electron microscopy under an accelerating voltage of 200 keV, and the average composition of the filtrates was tested by Inductively Coupled Plasma Optical Emission Spectrometer (ICP-OES, IRIS Intrepid II XSP, Thermo Fisher Corporation, USA).

The cathode consisted of 85 wt% active material, 5 wt% poly(vinylidene fluoride) as binder, and 10 wt% carbon black as conducting agent. After being blended in *N*-methylpyrrolidinone, the slurry was spread uniformly on aluminum foil and dried at 80 °C for 12 h in vacuum. A typical cathode disk contained active material of 3–4 mg cm^{-2}. Charge and discharge performance of the electrodes was evaluated using 2025 coin cells containing an electrolyte solution of 1M LiPF$_6$ in a mixed solvent of ethylene carbonate and dimethyl carbonate (1:1 volume ratio) in a Celgard 2320 micro-porous separator membrane. Lithium foil served as the counter electrode. The cells were assembled in an argon-filled glove-box (O$_2$ and H$_2$O levels <1 ppm). Galvanostatical charge and discharge was controlled between 2.0 and 4.8 V at a constant current density of 20 mA g^{-1} at room temperature (Xinwei CT3008W, Shenzhen Xinweier Electronic Co, China).

3 Results and discussion

3.1 Materials characterization

Figure 1 shows the powder X-ray diffraction patterns of the Li-Ni-Mn-O compounds prepared at 800 °C and 900 °C with different Li content. The structure of Li$_{1.18}$Ni$_{0.250}$Mn$_{0.572}$O$_2$(900) (Figure 1(a)) is primarily indexed based on the *R*-3*m* space group, which is the structure of the major layered component (LiNi$_{0.5}$Mn$_{0.5}$O$_2$) in similar materials. Some weak peaks between 20° and 25° of 2θ can be observed in the XRD patterns of the sample, which are considered to be caused by the short-range super-lattice ordering of Li, Ni, Mn in the transition metal layer. These peaks can be indexed to C2/*m* space group that characterizes Li$_2$MnO$_3$ [30]. Besides the two layered structures, the spinel phase of LiM$_2$O$_4$ (M=Ni, Mn) is also observed in Li$_{1.03}$Ni$_{0.277}$Mn$_{0.622}$O$_2$(900) and Li$_{1.05}$Ni$_{0.277}$Mn$_{0.642}$O$_2$(800),

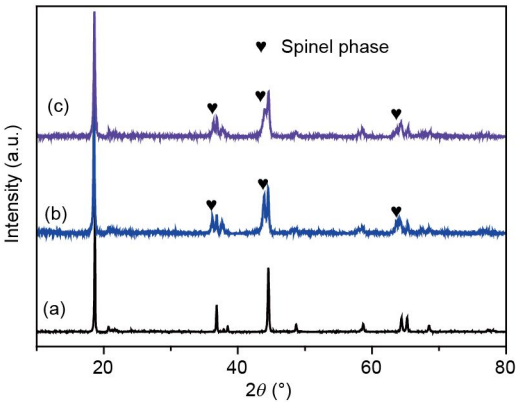

Figure 1 Powder XRD patterns of (a) Li1.18 (900), (b)Li1.03(900) and (c) Li1.05 (800).

which reflects the existence of a three-component composite electrode system (Figure 1(b) and (c)). The diffraction peak of spinel phase from $Li_{1.03}Ni_{0.277}Mn_{0.622}O_2$(900) is higher than that from $Li_{1.05}Ni_{0.277}Mn_{0.642}O_2$(800), which could be due to more Li_2O loss at higher temperature [31]. In this case, the higher calcinated temperature yields a more highly reduced spinel-like component in the composite electrode. So the content of spinel-phase is strongly dependent on the calcinating temperatures. According to the chemical composition results (Table 1), samples were nominated as $Li_{1.18}$(900), $Li_{1.03}$(900) and $Li_{1.05}$(800) respectively.

To attest the existence of spinel-phase, X-ray photoelectron spectroscopy (XPS) in the Mn_{2P} regions of the cathode material was utilized to examine the changes in valance state. The binding energy of each spectrum was calibrated using the C1s peak present from adventitious carbon (284.5 eV). The $Mn_{2p3/2}$ and $Mn_{2p1/2}$ peaks in the compound (Figure 2(a)) show BE (Binding Energy) of 642.7 and 654.2 eV respectively, which are in good agreement with values reported for Mn^{4+} in manganese oxide [32], while small shoulders appear in the signals (Figure 2(b, c)), indicating the existence of Mn^{3+} in $Li_{1.03}$(900) and $Li_{1.05}$ (800), where the mole ratio of Mn^{4+}/Mn^{3+} are 1.84 and 1.04 respectively. So there are more spinel phase component in $Li_{1.03}$(900) than that in $Li_{1.05}$ (800). In stark contrast to the Mn_{2p} spectrum, where the signal for multiple valences was affected by the Li content, the Ni_{2p} spectrum exhibits one stable oxidation state (not shown in this paper). The location of the signals for $2p_{1/2}$ and $2p_{3/2}$ states of Ni at 855.1, 860.9 and 872.8 eV, respectively, suggested an oxidation state of Ni^{2+} [33].

The typical microstructure of the 3 samples are shown in HRTEM image (Figure 3), which clearly shows the composite character of the powders with nano-domains of the layered-spinel components. Figure 3(a) shows layered fringes of Li(1.18) [34]. However, HRTEM images of Figure 3(b, c) show the remarkable coexistence of layered and spinel regions in which the close packed (001) planes of the layered Li_2MnO_3 component are aligned parallel to (111) planes of spinel component, confirming the fully integrated and composite character of their structure.

Figure 4(a–c) shows the particle morphologies of the three materials. The collected particles, composed of nano-sized primary particles, are all with spherical morphology. The size of primary particles (square shape) are between 100 nm and 400 nm, while the secondary particles are about 20 μm. Comparisons of Figure 4(a–c) illustrate that the overall particle shape and size were not essentially affected by the lithium content.

3.2 Electrochemical performances

The electrochemical performance of $Li_{1.18}$(900), $Li_{1.03}$(900) and $Li_{1.05}$(800) in a CR-2025 lithium cell is shown in Figure 5(a–c); the corresponding dQ/dV plots are shown in

Table 1 Compositions of the synthesized powders: (a) $Li_{1.18}$(900), (b)$Li_{1.03}$(900) and (c) $Li_{1.05}$(800)

Sample	Li/M (mole ratio)	Analyzed formula	Coulombic efficiency for the 1st cycle	Name
(a)	1.436	$Li_{1.18}Ni_{0.250}Mn_{0.572}O_2$	70.21%	$Li_{1.18}$(900)
(b)	1.146	$Li_{1.03}Ni_{0.277}Mn_{0.622}O_2$	93.95%	$Li_{1.03}$(900)
(c)	1.143	$Li_{1.05}Ni_{0.277}Mn_{0.642}O_2$	99.89%	$Li_{1.05}$(800)

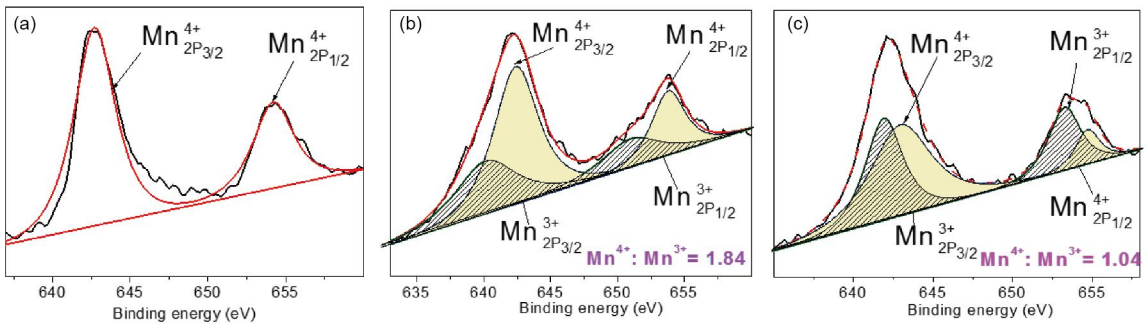

Figure 2 XPS spectra of the Mn_{2P} regions of (a) $Li_{1.18}$(900), (b)$Li_{1.03}$(900) and (c) $Li_{1.05}$(800).

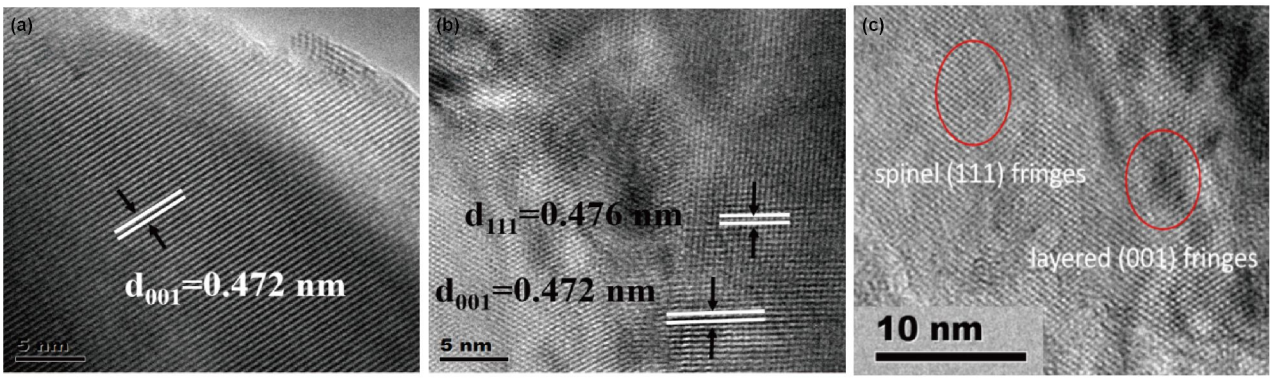

Figure 3 High-resolution TEM images of (a)$Li_{1.18}$(900), (b)$Li_{1.03}$(900) and (c)$Li_{1.05}$(800) showing the structural compatibility of layered and spinel domains.

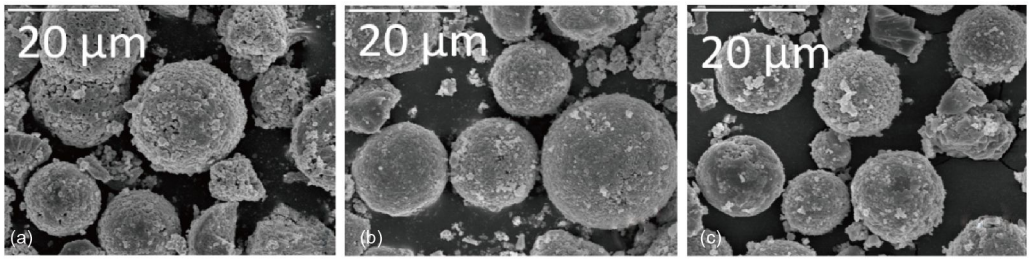

Figure 4 SEM images of (a) $Li_{1.18}$(900), (b)$Li_{1.03}$(900) and (c) $Li_{1.05}$(800).

Figure 6(a–c) respectively. The cells were initially charged to 4.8 V, discharged to 2 V, and then cycled between 2.0 and 4.8 V in the subsequent cycles at current density of 20 mA g^{-1}. The initial charging curve of $Li_{1.18}$(900) displays a voltage response typical of layered 'composite' $xLi_2MnO_3{\cdot}(1-x)LiNi_{0.5}Mn_{0.5}O_2$, showing two processes (Figure 5(a)), which can also be found in the dQ/dV plots in Figure 6(a): one is observed below 4.5 V, and the other is above 4.5 V. At the former process, the voltage increases monotonically, corresponding to the oxidation of Ni^{2+} to Ni^{4+}, until the potential reaches 4.5 V, and the latter results from the electrochemical removal of 'Li_2O' from the structure, correlating with the activation of Li_2MnO_3, which is responsible for the big irreversible capacity in the first cycle, if side contributions from electrode/electrolyte reactions are ignored. The irreversible capacity disappeared in the second and subsequent cycles, in agreement with the literature reports [35–37]. It is obvious that the dQ/dV plots show three distinct processes in the subsequent discharge: the peaks above 3.5 V can be assumed from the reduction of nickel (Ni^{4+}/Ni^{2+}); as the process below 3.5 V is attributed to the reduction of tetravalent manganese in the MnO_2-rich domains derived electrochemically from the Li_2MnO_3 component about 4.5 V. During the subsequent cycles, the reduction peak below 3.5 V grows and becomes evident, illustrating that the manganese redox reaction is progressively activated upon cycling. As a result, more and more tetravalent manganese ions participate in the electrochemical reactions and that is why the discharge capacity increases with cycles.

When the lithium content was decreased to yield integrated layered-spinel structures ($Li_{1.03}$(900)), the electrochemical processes become more complex in particular and several extra pairs of reversible peaks are observed. As shown in Figure 4(b), the shape of charge and discharge curves might be concerned with both spinel ($LiMn_2O_4$ or $LiNi_{0.5}Mn_{1.5}O_4$) and 'composite' layered electrode structures ($xLi_2MnO_3{\cdot}(1-x)LiNi_{0.5}Mn_{0.5}O_2$), which present several distinct regions, respectively; the corresponding dQ/dV plots are shown in Figure 5(b), in which the peaks were marked as A, B, C…respectively. Although it is difficult to identify the electrochemical participation of the layered and spinel components unequivocally, based on the dQ/dV plots of $Li_{1.18}$(900) and other related studies [26], the complexity of the electrochemical processes can be predominantly assigned either to the layered component, to the spinel component, or to both components: the small peak B at 4.5 V results from the electrochemical removal of "Li_2O" from the structure of 'Li_2MnO_3'; moreover, the peaks C & D (divided in two peaks) are associated with the typical $LiNi_{0.5}Mn_{1.5}O_4$ (Ni^{2+}/Ni^{3+}/Ni^{4+}); while peaks A, E & F might involve the participation of the spinel ($LiMn_2O_4$) and layered type ($LiNi_{0.5}Mn_{0.5}O_2$) composite electrodes; peaks G & I are the characteristic features of the reduction of tetravalent manganese in the MnO_2-rich domains derived electrochemically from the Li_2MnO_3 component about 4.5 V (peak B); the redox peaks H & I are related with the reversible spinel phase ($LiNi_{0.5}Mn_{1.5}O_4$ or $LiMn_2O_4$) to rocksalt $Li_2Ni_{0.5}Mn_{1.5}O_4$ or $Li_2Mn_2O_4$, in which lithium ions are inserted into the

octahedral sites with the concomitant oxidation-reduction reaction of Mn^{3+}/Mn^{4+}. Notice that several peaks (such as A and H) become increasingly larger on further cycling, but there might be different reasons. Peaks A, F, G & I originate from the manganese redox reaction in the activated manganese derived from the Li_2MnO_3 component, which is progressively activated upon cycling, while the structure has slowly transformed from spinel to rocksalt during insertion/extraction of lithium ions in peaks G and H. It is speculated that the increased electrochemical capacity can be partly attributed to the activation of tetravalent manganese in Li_2MnO_3 and partly to the formation of $Li_2Ni_{0.5}Mn_{1.5}O_4$ or $Li_2Mn_2O_4$. As we can see in Figure 5(c) and 6(c), the charge and discharge curves of $Li_{1.05}(800)$ present the same electrochemical processes as $Li_{1.03}(900)$, which shows that there is more 'composite' layered phase in $Li_{1.05}(800)$, in agreement with the results of XRD (Figure 1). It is obvious that the reduction peaks move to lower voltage region, while

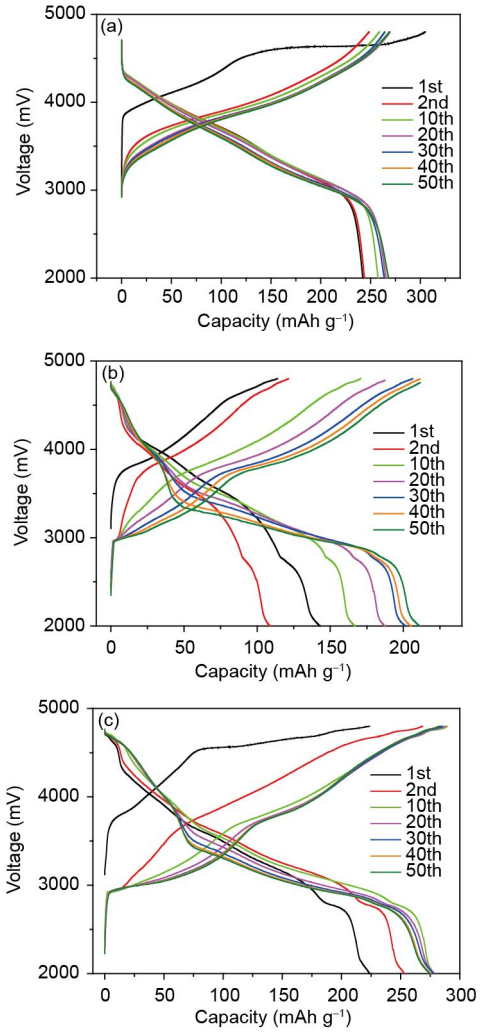

Figure 5 Charge/discharge profiles for the 1st, 2nd, 10th, 20th, 30th, 40th and 50th cycles of lithium cells with: (a) $Li_{1.18}(900)$, (b)$Li_{1.03}(900)$ and (c) $Li_{1.05}(800)$.

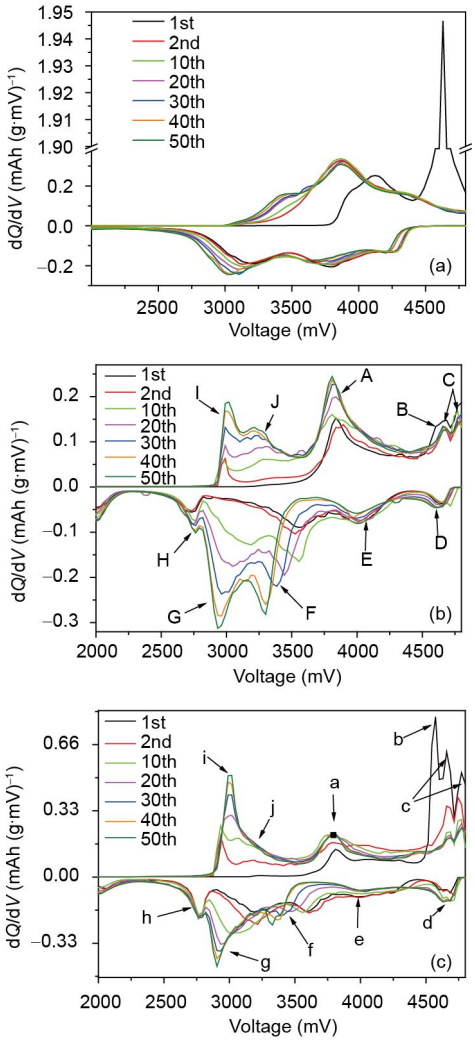

Figure 6 dQ/dV plots for the 1st, 2nd, 10th, 20th, 30th, 40th and 50th cycles (delivered between 2.0 and 4.8 V at 20 mA g^{-1}) of lithium cells with: (a) $Li_{1.18}(900)$, (b)$Li_{1.03}(900)$ and (c) $Li_{1.05}(800)$.

the oxidation peaks shifts to the higher voltage region during the cycling stage, which can be concluded that there might be some structure transformation in the electrode materials.

The existence of spinel-like phase in $Li_{1.03}(900)$ and $Li_{1.05}(800)$ eliminates the first cycle, irreversible capacity loss that is observed for $Li_{1.18}(900)$, as illustrated in Table 1. For the two component composite structure $xLi_2MnO_3{\cdot}(1{-}x)LiMO_2$ (M=Mn, Ni, Co), two lithium ions extract from the Li_2MnO_3 component during the first charge, while only one lithium per MnO_2 unit embeds into the lattice during first discharge, so this material undergoes a huge irreversible capacity loss in the first cycle. As to $Li_{1.03}(900)$ and $Li_{1.05}(800)$, when discharged to 2.8 V, the spinel-like component serves as a host to insert the extracted lithium-ions that could not be inserted back into the layered oxide lattice, which eliminates the irreversible capacity loss during the first cycle, as well as improving specific capacities to some extent.

Figure 7 described the specific capacity vs. cycle number plots for the first 50 cycles of the lithium cells when cycled between 4.8 V and 2.0 V at current density of 20 mA g^{-1}. The sample $Li_{1.18}$(900) had a discharge capacity of about 242 mAh g^{-1} at the initial cycle (in Figure 7(a)), and the reversible capacity was also 262 mAh g^{-1} at the 50th cycle, exhibiting good cycling performance. Although the initial discharge capacity was only 107 mAh g^{-1} delivered by $Li_{1.03}$(900), the subsequent capacity of the cell increased steadily to 212 mAh g^{-1} after 50 cycles (shown in Figure 7(b)), when the full capacity of the spinel and layered electrodes can be exploited over the wide voltage window. Although $Li_{1.05}$(800) presents the same electrochemical processes as $Li_{1.03}$(900), it shows different cycling performances (Figure 7(c)). By contrast, $Li_{1.05}$(800) yielded an initial capacity of 223 mAh g^{-1} that increased to 280 mAh g^{-1} step by step during the first five cycles, and very high discharge capacity and excellent cycling stability were obtained. According to the results above, we could infer that the cubic spinel-like phase, which is helpful to improve the first cycle coulombic efficiency and specific capacity, may impede the lithium-ion diffusion in the lithium layer and degrade the electrochemical performance of the layered phases largely [38]. When the calcinated temperature was changed to 800 °C, the content of spinel-like phase in $Li_{1.05}$(800) decreased, so that the first discharge capacity of $Li_{1.05}$(800) (223 mAh g^{-1}) is much more than that of $Li_{1.03}$(900) (107 mAh g^{-1}). When the transformation of spinel-like phase to rocksalt phase becomes more obvious with cycling, the more lithium-ions can be extracted from the matrix, resulting in the increase of specific capacity during cycling.

According to the discussion above, the existence of spinel-like phase eliminates irreversible capacity loss during the first cycle and improves specific capacity to some extent, when discharged to 2.8 V. However, the specific capacity and cycle stability are affected largely by content of cubic sipnel-like phase, which can be controlled by the lithium content in the electrode material.

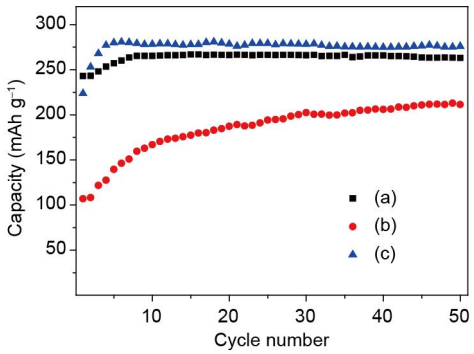

Figure 7 Specific capacity (delivered between 2.0 and 4.8 V at 20 mA g^{-1}) vs. cycle number for lithium ion cells with: (a) $Li_{1.18}$(900), (b)$Li_{1.03}$(900) and (c) $Li_{1.05}$(800).

4 Conclusions

In this work, the lithium content in $0.4Li_2MnO_3 \cdot 0.6LiNi_{0.5}Mn_{0.5}O_2$ was decreased to yield integrated layered-spinel structures, and the existence of spinel-like phase eliminates the irreversible capacity loss completely in the first cycle. The elimination is due to the ability of spinel phase to insert the extracted lithium-ions that could not be inserted back into the 'composite' layered structure $0.4Li_2MnO_3$-$0.6LiNi_{0.5}Mn_{0.5}O_2$ when discharged to 2.8 V. The $Li_{1.05}Ni_{0.277}Mn_{0.642}O_2$(800) composite calcinated at 800 °C exhibits a high capacity (about 275 mAh g^{-1} at 0.1 C) with little or no irreversible capacity loss in the first cycle and good cycling performance. The composite strategy presented here offers an attractive method to increase the first cycle coulombic efficiency to almost 100% of Li-rich materials. However, the cubic spinel-like phase may impede the lithium-ion diffusion in the lithium layer and degrade the electrochemical performance of the layered phases largely, so the content of cubic spinel-like phase must be controlled to enhance the electrochemical performance of the integrated layered-spinel materials.

Acknowledgments Financial support by the National Basic Research Program of China (2009CB220105) and Beijing Natural Science Foundation (2120001) is gratefully acknowledged.

Conflict of interest The authors declare that they have no conflict of interest.

1 Whittingham MS. *Chem Rev*, 2004, 104: 4271–4302
2 Belharouak I, Lu W, Vissers D, Amine K. *Electrochemistry Commun*, 2006, 8: 329–335
3 Abouimrane A, Compton OC, Deng H, Belharouak I, Dikin DA, Nguyen SBT, Amine K. *Electrochem Solid-State Lett*, 2011, 14: A126
4 Kim MG, Jo M, Hong YS, Cho J. *Chem Commun*, 2009, 218–220
5 Croguennec L, Bains J, Ménétrier M, Flambard A, Bekaert E, Jordy C, Biensan P, Delmas C. *J Electrochem Soc*, 2009, 156: A349
6 Gao J, Kim J, Manthiram A. *Electrochemistry Commun*, 2009, 11: 84–86
7 Jarvis KA, Deng Z, Allard LF, Manthiram A, Ferreira PJ. *Chem Mater*, 2011, 23: 3614–3621
8 Grey CP, Yoon WS, Reed J, Ceder G. *Electrochem Solid-State Lett*, 2004, 7: A290
9 Grey CP, Dupré N. *Chem Rev*, 2004, 104: 4493–4512
10 Yoon WS, Iannopollo S, Grey CP, Carlier D, Gorman J, Ceder G. *Electrochem Solid-State Lett*, 2004, 7: A167
11 Lu Z, Dahn JR. *J Electrochem Soc*, 2002, 149: A815
12 Armstrong AR, Holzapfel M, Novak P, Johnson CS, Kang S, Thackeray MM, Bruce PG. *J Am Chem Soc*, 2006, 128: 8694–8698
13 Rossouw M, Thackeray M. *Mater Res Bull*, 1991, 26: 463–473
14 Rossouw MH, Liles DC, Thackeray MM. *J Solid State Chem*, 1993, 104: 464–466
15 Tang W, Kanoh H, Yang X, Ooi K. *Chem Mater*, 2000, 12: 3271–3279
16 Paik Y, Grey CP, Johnson CS, Kim JS, Thackeray MM. *Chem Mater*, 2002, 14: 5109–5115

17 Kang SH, Johnson CS, Vaughey JT, Amine K, Thackeray MM. *J Electrochem Soc*, 2006, 153: A1186
18 Myung ST, Izumi K, Komaba S, Yashiro H, Bang HJ, Sun YK, Kumagai N. *J Phys Chem C*, 2007, 111: 4061–4067
19 Myung ST, Izumi K, Komaba S, Sun YK, Yashiro H, Kumagai N. *Chem Mater*, 2005, 17: 3695–3704
20 Kang YJ, Kim JH, Lee SW, Sun YK. *Electrochim Acta*, 2005, 50: 4784–4791
21 Tan K, Reddy M, Rao G, Chowdari B. *J Power Sources*, 2005, 141: 129–142
22 Zheng JM, Li J, Zhang ZR, Guo XJ, Yang Y. *Solid State Ionics*, 2008, 179: 1794–1799
23 Xia Y. *J Electrochem Soc*, 1997, 144: 2593
24 Zheng J, Deng S, Shi Z, Xu H, Xu H, Deng Y, Zhang Z, Chen G. *J Power Sources*, 2013, 221: 108–113
25 Gao J, Kim J, Manthiram A. *Electrochemistry Commun*, 2009, 11: 84–86
26 Wu Y, Vadivel Murugan A, Manthiram A. *J Electrochem Soc*, 2008, 155: A635
27 Gao J, Manthiram A. *J Power Sources*, 2009, 191: 644–647
28 Xia Y, Sakai T, Fujieda T, Yang XQ, Sun X, Ma ZF, McBreen J, Yoshio M. *J Electrochem Soc*, 2001, 148: A723
29 Kim JS, Johnson CS, Vaughey JT, Thackeray MM, Hackney SA, Yoon W, Grey CP. *Chem Mater*, 2004, 16: 1996–2006
30 Koga H, Croguennec L, Mannessiez P, Ménétrier M, Weill F, Bourgeois L, Duttine M, Suard E, Delmas C. *J Phys Chem C*, 2012, 116: 13497–13506
31 Abouimrane A, Compton OC, Deng H, Belharouak I, Dikin DA, Nguyen SBT, Amine K. *Electrochem Solid-State Lett*, 2011, 14: A126
32 Thackeray MM, Kang SH, Johnson CS, Vaughey JT, Benedek R, Hackney SA. *J Mater Chem*, 2007, 17: 3112
33 Ammundsen B, Paulsen J. *Adv Mater*, 2001, 13: 943–956
34 Yabuuchi N, Yoshii K, Myung ST, Nakai I, Komaba S. *J Am Chem Soc*, 2011, 133: 4404–4419
35 Johnson CS, Kim JS, Lefief C, Li N, Vaughey JT, Thackeray MM. *Electrochemistry Commun*, 2004, 6: 1085–1091
36 Robertson AD, Bruce PG. *Electrochem Solid-State Lett*, 2004, 7: A294
37 Park S, Kang S, Johnson C, Amine K, Thackeray M. *Electrochemistry Commun*, 2007, 9: 262–268
38 Yu H, Kim H, Wang Y, He P, Asakura D, Nakamura Y, Zhou H. *Phys Chem Chem Phys*, 2012, 14: 6584